

A shape optimization approach towards improving the

*1 Shape optimization for improved
2 understanding of magmatic plumbing
3 systems*

4 Théo Perrot, Freysteinn Sigmundsson

5 June 2024

6 Abstract

*7 In volcano geodesy, inverse problems caused by identifying the location and
8 shape of magmatic bodies based on ground deformation data are common.
9 Traditional approaches often rely on models with predefined shapes, which
10 can limit their accuracy. To address this, we present a shape optimisation
11 method using a level-set approach that flexibly determines the optimal
12 shape of a magma chamber without prior shape assumptions. By minimising
13 the discrepancy between observed and modelled surface displacements,
14 our adapted algorithm becomes suitable for solving inverse volcano deforma-
15 tion problems. We explore the capabilities of this approach with synthetic
16 data and apply it to InSAR observations of the Svartsengi volcanic system in
17 Iceland, demonstrating its potential to improve volcanic hazard assessment
18 after maturation through future work.*

*The article is devoted to an inverse problem in volcano geodesy,
whose main target is to identify the location and shape of
magmatic chambers based on ground data measurement.*

¹⁹ **1 Introduction**

²⁰ **1.1 Challenge**

²¹ In volcano geodesy, inverse problems are central to estimating the position
²² of magmatic bodies using ground motion as a proxy. Displacement is ob-
²³ served by geodetic measurements such as Global Navigation Satellite System
²⁴ (GNSS) point positioning, leveling campaigns, or Synthetic Aperture Radar
²⁵ (InSAR) interferometry within a volcanic field, and the subsurface processes
²⁶ causing the movement are inferred from these observations (Dzurisin 2007).
²⁷ Magmatic sources are modeled as pressurized cavities that deform the sur-
²⁸ rounding host rocks and cause the surface to move. Various inversion meth-
²⁹ ods based on parametric analytical or numerical models aim at finding the
³⁰ optimal values for the vector of d free parameters $\vec{m} \in \mathbb{R}^d$ of the model. Then
³¹ an error function $J(\vec{m})$ is representative of the misfit between the observed
³² displacements and the prediction of the model. \vec{m}_{opt} can then be found using
³³ various inversion techniques that minimize J : global optimization based on
³⁴ analytic (Cervelli et al. 2001) or numerical models (Hickey and Gottsmann
³⁵ 2014, Charco and Galán del Sastre 2014), Bayesian inference (Bagnardi and
³⁶ Hooper 2018, Trasatti 2022), or genetic algorithms (Velez et al. 2011) on
³⁷ analytic models. The choice of the method is constrained by the reasonable
³⁸ number of evaluations of $J(\vec{m})$: numerical models handle a complex descrip-
³⁹ tion of the system, but are computationally expensive compared to analytic
⁴⁰ models, which on the other hand may lead to an oversimplification (Taylor,
⁴¹ Johnson, and Herd 2021).

⁴² However, each of these finite-dimensional optimization methods is limited
⁴³ by the intrinsic assumption of a definite parametric shape for the source. In
⁴⁴ fact, analytic expressions can be derived for only a few regular shapes such as
⁴⁵ point source (Mogi 1958), finite sphere source (McTigue 1987), or ellipsoidal
⁴⁶ source (Yang, Davis, and Dieterich 1988), and any numerically generated
⁴⁷ shape must be parameterized to be inverted. Even in the case where complex
⁴⁸ shapes are chosen, they would require additional describing parameters, and
⁴⁹ ultimately any of the above methods may face the curse of dimensionality.
⁵⁰ The goal of this paper is not to give a definitive answer to these limitations,
⁵¹ but rather to lay the first stone for a new approach that overcomes these
⁵² difficulties.

⁵³ **1.2 Shape optimization**

⁵⁴ Shape ~~and topology~~ optimization aims to find the shape that minimizes a
⁵⁵ given function defined on a given system, without the need for prior assump-

as in data, nonrigid under constraints.

in analytical field now

where can we be

56 ~~tions about shape and topology~~. It is actively developed by part of the applied
57 mathematics community and is widely used in engineering to find optimal
58 designs for systems. In structural mechanics, to maximize the stiffness of a
59 solid structure such as a cantilever beam (Bendsøe and Ole Sigmund 2004),
60 in fluid-structure interaction on heat exchangers or flying obstacles (F. Feppon et al. 2020), and even as a way to explore new architecture for buildings
61 (Beghini et al. 2014). Most finite element simulation and design software now
62 implements ~~a~~ an embedded shape optimization module (Frei 2015, Slavov and
63 Konsulova-Bakalova 2019, Le Quilliec 2014). However, its use has not yet
64 been reported in the context of inverse problems in volcano geodesy, where
65 it can overcome the shape hypothesis problem as long as an internal pressure
66 value is assumed.

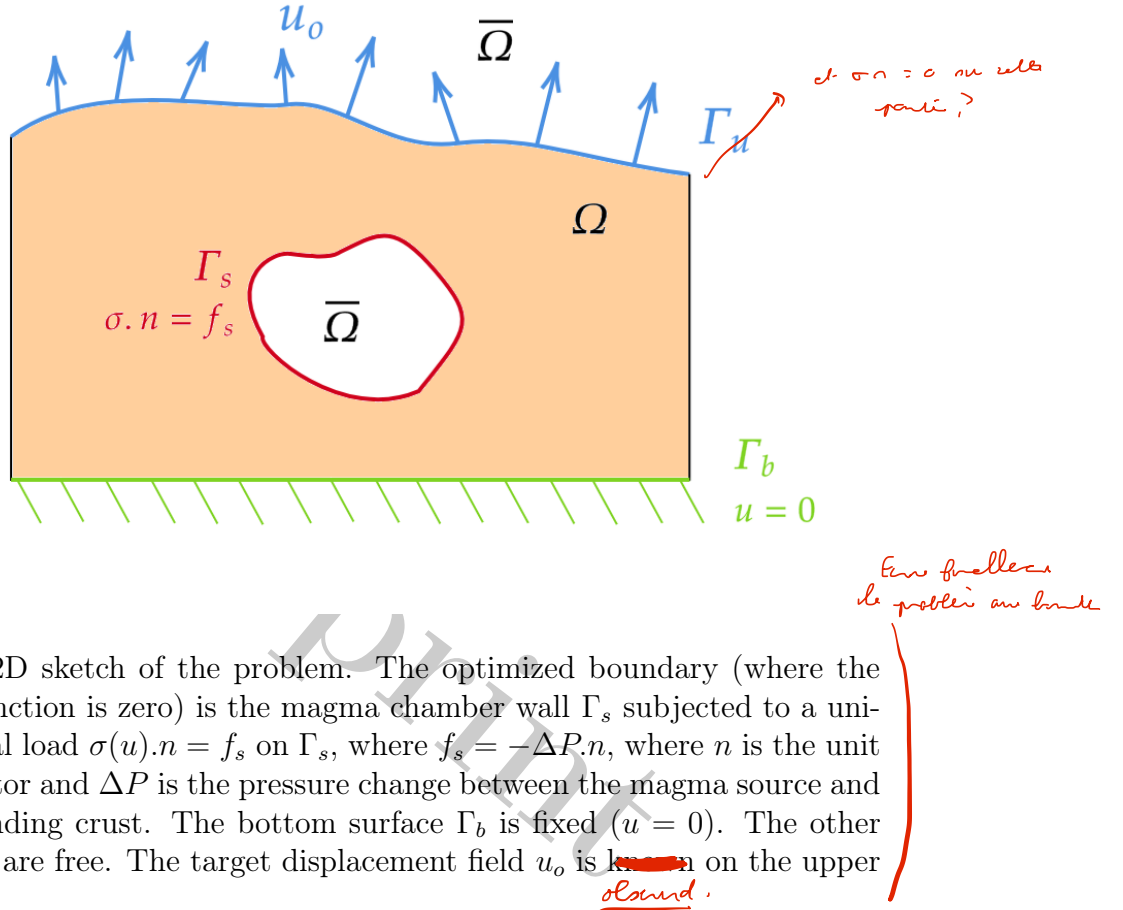
→ Ansys,
Altair,
Cimat...
...

68 Many paradigms coexist in shape optimization as reviewed by Ole Sig-
69 mund and Maute 2013, one of the most popular being SIMP optimization,
70 where a density value is optimized for each element of the mesh with values
71 between 0 (void) and 1 (material) before being black and white filtered to
72 output a design (O. Sigmund 2001, Bendsøe and Ole Sigmund 2004), with
73 several open source implementations (Andreassen et al. 2011, Hunter et al.
74 2017). We chose level-set shape optimization instead because it has the ad-
75 vantage of providing an explicit representation of the boundary at each step
76 of the optimization, which is crucial for us as explained later (section 2). For
77 this, we relied on the work of Dapogny and Florian Feppon 2023, who thor-
78oughly described and vulgarized the method, as well as providing a freely
79 available open source implementation of the method, `sotuto`(Dapogny and
80 Florian Feppon 2024), which we modified and extended to adapt it to inverse
81 geodetic problems.

82 2 Method

83 Here we briefly present the key ingredients of level set shape optimization
84 along with their implications for our problem. The full mathematical back-
85 ground on which it relies is not detailed, but see this chapter by Allaire,
86 Dapogny, and Jouve 2021 for a comprehensive ~~and rigorous~~ step by step description sup-
87 ported by proofs and theorems. It is also worth noting that many aspects
88 of secondary importance to the method are not mentioned for the sake of
89 brevity. For the unfamiliar reader interested in understanding the method,
90 the lecture (especially part III) given by Dapogny and Bonnetier 2024 at the
91 Université Grenoble Alpes is also recommended.

92 2.1 Model



93 Let Ω be a bounded domain of \mathbb{R}^3 whose shape we want to optimize
 94 by modifying parts of its boundary $\partial\Omega$. As for classical analytical mod-
 95 els of volcanic deformation induced by magmatic activity, Ω is a domain
 96 representing a portion of the shallow Earth crust, including the volcano, as-
 97 sumed to be homogeneous, isotropic, and elastic. The governing equations
 98 are $-\operatorname{div}(Ae(u)) = 0$ in Ω , where $e(u)$ is the strain tensor of the displace-
 99 ment field u and A is the constitutive law tensor, $Ae = 2\mu e + \lambda \operatorname{tr}(e)Id$ for linear
 100 elasticity. Boundaries under different conditions, see Fig. 1 for all notations.

101 The part of $\partial\Omega$ to be optimized is Γ_s , the boundary of the magma chamber,
 102 which is modeled as an empty, uniformly pressurized cavity. Therefore, a
 103 value for the internal pressure P_{int} must be assumed (see Discussion for devel-
 104 opment). In the following text we talk about optimizing $\partial\Omega$, but in practice

sigmā conn a u, orni

A dien yus pained

105 only $\Gamma_s \subset \partial\Omega$ is of interest and will be modified, any other boundary will be
 106 fixed during the iterations.

107 We want to find $\partial\Omega$ such that the displacement of the model $u(\Omega)$ is as
 108 close as possible to the observed displacement u_o on the surface Γ_u . Thus,
 109 the unconstrained shape optimization problem we want to solve is the mini-
 110 mization of a squared RMS discrepancy

$$\min_{\Omega} J(\Omega) = \int_{\Gamma_u} (u(\Omega) - u_o)^2 dS \quad (1)$$

111 2.2 Hadamard Boundary Variation

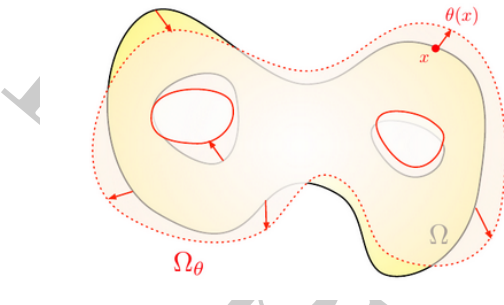


Figure 2: Reproduced from Allaire, Dapogny, and Jouve 2021

is merged with Ω₀

112 Overall, this method can be considered a classical iterative gradient de-
 113 scent algorithm. J is first initialized at J_0 with an instructed first guess
 114 for Ω_0 and then iteratively decreased by moving $\partial\Omega$ of a given step in a
 115 given descent direction $\theta : \mathbb{R}^3 \mapsto \mathbb{R}^3 \in W^{1,\inf}$ (the Sobolev space of uni-
 116 formly bounded functions, Allaire, Dapogny, and Jouve 2021) chosen using
 117 the shape derivative $J'(\Omega)(\theta)$. *correct?* *underlies*

118 The boundary variation method of Hadamard 1908 introduces the notion
 119 of shape differentiation $F'(\Omega)(\theta)$ of a functional F defined on Ω in the di-
 120 rection θ . In short, such a derivative is based on the variation of a bounded
 121 domain $\Omega \mapsto \Omega_\theta := (Id + \theta)(\Omega)$: the surface $\partial\Omega$ is slightly moved according
 122 to a small vector field $\theta(x)$, as shown in Fig. 2. Once such a derivative
 123 exists, one can compute a descending direction at the n^{th} step θ_n , such as
 124 $J'(\Omega)(\theta_n) \leq 0$, so $J_{n+1} \leq J_n$, to decrease the value of J at each iteration.

125 In our case, after derivation based on the Cea 1986 formal method, we
 126 found under the variational form :

$$J'(\Omega)(\theta) = \int_{\Gamma_s} \left(Ae(u) : e(p) + \frac{\partial f_s}{\partial n} p + \frac{\partial p}{\partial n} f_s + \kappa f_s p \right) . \theta . ndS \quad (2)$$

5 *Combien de paramètres Δp ?*

127 where $\kappa = \operatorname{div}(n)$ is the mean curvature at the boundary, and p is the
 128 adjoint solution of $\text{div } p = 0$.

$$\forall v \in H^1(\mathbb{R}^3), \int_{\Gamma_u} 2(u_\Omega - u_o)v dS + \int_{\Omega} Ae(v) : e(p) dV = 0 \quad (3)$$

and $p = 0$ on Γ_b

129 From there, we can trivially move Ω in the direction $\theta = -A$ (where
 130 A is the integrand term in parentheses) to ensure that $J'(\Omega)(\theta) \leq 0$. This
 131 guarantees that $J(\Omega_{n+1}) \leq J(\Omega_n)$: the series $J(\Omega_n)$ converges to a minimum.

132 2.3 Level-set representation

133 A key issue is the representation of the surface to be optimized. The level
 134 set method allows to track dramatic changes as well as topology variations
 135 (creation of new holes). A certain function $\phi : D \mapsto \mathbb{R}$ is defined over the
 136 domain $D \in \mathbb{R}^3$ in such a way that the shape boundary is the level set 0,
 137 i.e. reads $\partial\Omega = \phi(x = 0)$. Basically, ϕ can be taken as the signed distance
 138 between any point x and $\partial\Omega$, as shown in the example fig. 3. In this way,
 139 $\partial\Omega$ is implicitly manipulated when transforming ϕ .

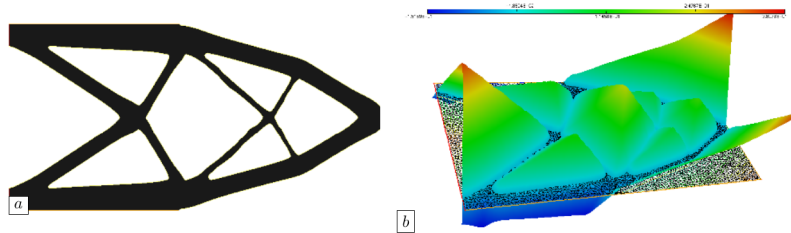


Figure 3: Reproduced from Dapogny and Florian Feppon 2023

140 Ω_n is then deformed by advecting the corresponding ϕ_n with a velocity
 141 field $V(x) = \tau_n \theta_n$, where τ_n is the additional step size. The advection equa-
 142 tion usually appears in fluid mechanics to describe the evolution of a quantity
 143 transported by a given velocity field, but here there is a smooth and flexible
 144 way to modify ϕ which ensures smoothness of Ω_{n+1} and change of topology
 145 (see Allaire, Dapogny, and Jouve 2021).

Que va-t-il se passer ?

146 2.4 Numerical implementation

147 In practice, the D domain is discretized into a mesh T_n on which each vari-
 148 ational form is solved at each iteration n . This includes the solution of the

149 elasticity to get u_n , the adjoint state p_n , the computation of the shape gradient J'_n , the descent direction θ_n , the advection of ϕ_n . In **sotuto** it is achieved
150 by calling scripts written in FreeFem++, a finite element software that allows
151 solving any integral form of elliptic PDE (Hecht 2012).

152 Once the new ~~shape~~ Ω_{n+1} is computed and discretized thanks to a local
153 remeshing phase, a new evaluation of J^{n+1} is performed. Since τ is arbitrarily
154 fixed and initialized to 1, it can happen that Ω_n is shifted by too large a step
155 and so $J_{n+1} \geq J_n$. To adjust the step size, a line search procedure is
156 implemented and adjusts the step size by decreasing it if the new iteration
157 is the worst to ensure an improvement of J by computing a new Ω_{n+1} being
158 a less deformed version of Ω_n . On the contrary, if Ω_{n+1} is accepted, τ is
159 increased to speed up convergence. A tolerance is set to accept iterations if
160 the increase in J is reasonable.

161 The global optimization loop has no termination criterion. Thus, it is up
162 to the user to stop it when no significant improvement in J can be achieved,
163 or when the shape is not realistic.

164 The loop and the line search are implemented in Python in **sotuto**. Then
165 the FreeFem scripts are called by the Python script core and data is ex-
166 changed via temporary files.

167 The above aspects are implemented in **sotuto**. However, we extended its
168 functionality to handle our geophysical problem, in a fork we called **magmaOpt**.
169 This includes ~~scripts~~: scripts to create the domain and initial source with a flexible
170 mesher GMSH which handle complex geometries such as the one generated
171 by topography Geuzaine, Remacle, and Dular 2009 ,adapting FreeFem scripts
172 to different error functions, allowing optimization of the loaded boundary Γ_s
173 and so on.

175 3 Validation with synthetic data

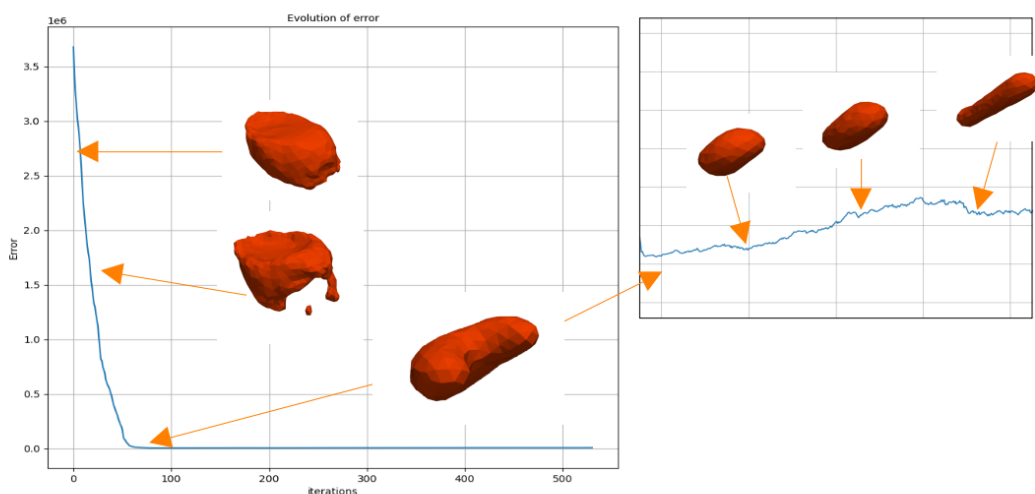
176 To test the method, the idea is to do a kind of cross-validation. On the
177 one hand, we form synthetic observation data from a known source. On
178 the other hand, we initialize ~~the~~ the algorithm with a first guess for the source
179 shape and location. We expect the algorithm to iteratively modify the shape
180 of the source and converge to the correct shape and location. In fact, the
181 3D location of the source (e.g., its center of gravity for a random shape) is
182 not directly optimized as a vector of discrete parameters, but is modified by
183 the simple fact that the boundary is free to move in any direction, and thus
184 can take on a kind of "average rigid body motion" as it gradually moves the
185 center in a given direction.

186 In practice, the synthetic observed surface displacement field is derived

187 from the McTigue 1987 solution, an analytical approximation of the displacement caused by a uniformly pressurized spherical cavity (the magma domain) embedded in an isotropic, homogeneous, and planar elastic medium (the host crust) with elastic constants $\text{tp } E = 10\text{GPa}$ and $\mu = 0.25$.

191 Usually, the quantities to be determined with parametric inversion based
 192 on a McTigue model are the location and the radius. The pressure change
 193 can also be left as a free parameter, but is interchangeable with the radius,
 194 so one must be fixed to determine the other, see (Greiner 2021) for more
 195 details. For the synthetic source, we fixed these free parameters to $z = -5\text{km}$,
 196 $\Delta P = 10\text{MPa}$, $R = 1.5\text{km}$, which are typical values for inverted magmatic
 197 domains.

198 `magmaOpt` is then allowed to run freely, without any termination condition,
 199 to see whether or not it succeeds in converging from the ellipsoid to the
 200 McTigue sphere we used to generate the synthetic displacement.



201 Figure 4: Evolution of error and successive ~~sphere~~ shapes taken by the magma
 202 source during an optimization loop. The initial guess is a flat ellipsoid of
 203 semi-axes $r_x = 2\text{km}$, $r_y = 3\text{km}$, $r_z = 1\text{km}$
 204 centered on the true spherical source. The minimum is reached at iteration
 205 82.

201 As shown in the figure 4, the algorithm seems to converge to a minimum.
 202 After that, the slope of the cost function is positive because a small increase
 203 in J is allowed. It is obvious that no other minima are found, as the shape
 204 evolves towards a stick-shaped feature, far from the expected solution. We
 205 can also discuss the minima found. The surface reached is obviously not a

206 sphere, but it is closer than any shape found before. We expect the shape to
 207 be closer to a sphere with a finer mesh defined. Many improvements could be
 208 realized: for example, once it is obvious that the algorithm will not converge
 209 to a better solution, we could restart the algorithm on the best solution
 210 found, set new evolution parameters, and allow a finer mesh. By repeating
 211 this process automatically, it may be possible to arrive at a more likely shape
 212 for the magma reservoir.

213 4 Real test case : Svartsengi 2022 inflation

214 We now apply the method to infer the shape of a magma domain in a recent
 215 period of volcanic unrest and eruption in SW Iceland by evaluating the shape
 216 of a magma body responsible for the ground inflation observed from 21 April
 217 to 14 June 2022 at Svartsengi on the Reykjanes peninsula. This is one of
 218 5 inflation episodes that preceded catastrophic dike breaches and eruptions
 219 at the Sundhnúkur crater row, which caused the destruction of the city of
 220 Grindavík (Sigmundsson et al. 2024).

221 The observational data used are the line-of-sight (LOS) displacement
 222 maps of the area from Cosmo SkyMed available in Parks et al. 2024, the
 223 data used in Sigmundsson et al. 2024. After uniform downsampling and
 224 mesh reprojection (the data points must be aligned on the mesh nodes), the
 225 ascending A32 and descending D132 tracks were both used in the RMS error
 226 function we adapted to the LOS geometry.

$$J(\Omega) = \sum_{i \in tck} \alpha_i \int_{\Gamma_u} (L_i(u(x)) - l_o^i(x))^2 dS \quad (4)$$

227 Where $tck = \{A125, D132\}$. For each track i , α_i is the weight of the track
 228 ($\forall i, \alpha_i = 1$ here), $L_i : \mathbb{R}^3 \mapsto \mathbb{R}$ is the function that projects the 3D sur-
 229 face displacement given by the model into the LOS geometry, and l_o^i is the
 230 observed LOS displacement.

231 We then used the framework developed above, only projecting the InSAR
 232 data onto the mesh of D and modifying the expression of the error function
 233 in `magmaOpt`.

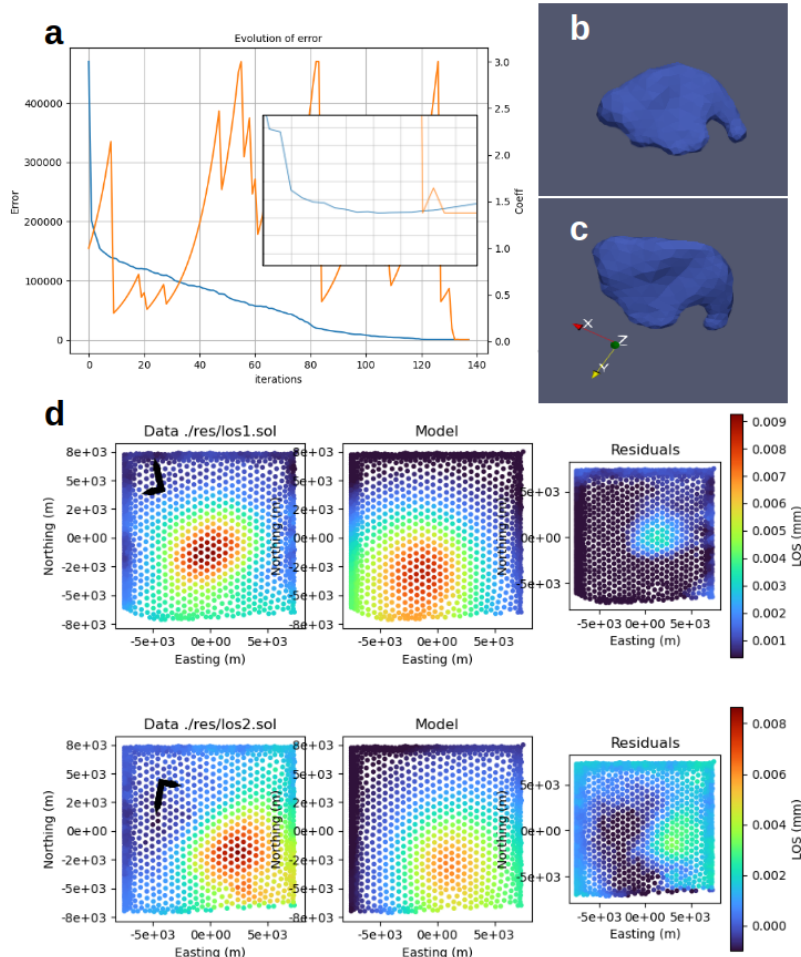


Figure 5: a) Convergence plot with embedded zoom. The blue line is the error and the orange line is the evolution of τ . Minima are reached at iteration 128. b,c) Side and top view of the source Γ_s minimizing J . d) Data, model and residuals of the LOS displacements at iteration 128 for the two InSAR tracks A32 (top) and D132 (bottom). Black arrows are heading and looking directions, coordinates are ISN16 **islands** shifted to a local origin (2529373E, 179745N).

The results shown in figure 5 are encouraging: after providing an initial guess located at the center of inflation at depth for a sphere of radius RR, the algorithm is able to iteratively change the shape and depth of the magma domain to finally result in a sill-like flattened spheroid whose centroid is located at DD depth. This is consistent with the presumed depth found in the supporting information of Sigmundsson et al. 2024, which performs an

240 analytical model-based inversion. Although the pressure must be fixed, as
241 explained in 1.2, the result can be used to compare the final shape of the
242 magmatic intrusion and give a richer insight into it. Here we see interesting
243 features, such as an increasing thickness on the north side, that can't
244 be traced by any other method. The algorithm produces features that we
245 consider to be artifacts, probably due to mesh refinement problems, such as
246 small holes or horn-shaped features.

247 5 Discussion

248 This work paves the way for a new class of methods that tackle an unknown
249 geometry of the magmatic domains, thus giving the possibility to explore
250 irregular shapes that are more likely to exist compared to any other usually
251 assumed regular shapes. However, even if the first results presented are
252 promising, many questions remain to be answered. First of all, the internal
253 pressure of the chamber must be specified, which is a strong hypothesis.
254 In this context, the precise shape of the source should be determined as a
255 second step. The traditional analytical model-based inversion would be run
256 first, giving a pressure and a first educated guess for the position and shape
257 of Ω_0 . Then a more realistic shape could be sought with a shape optimization
258 taking the output of the inversion as an initial guess.

259 Adding constraints may also be an interesting way to explore. For ex-
260 ample, the volume of the source could be constrained to be within bounds
261 or even to match a certain value. The implemented shape optimization is
262 certainly able to handle constraints as described by [allaire202](#). The physical
263 meaning of the best shape might benefit from a more constrained problem,
264 and the less influencing deeper part of the source might be less random.

265 To better understand the influence of data partitioning and variablitiy,
266 additional tests could be run with synthetic data. We can think of tests
267 such as masking part of the surface displacement field, introducing noise
268 and parasitic signals, reducing the number of data points, as is often the
269 case in reality with areas of volcanic systems lacking data coverage (glacier,
270 river, lava, forest) and subjected to perturbations (atmospheric distortion,
271 weather).

272 It is also important to mention that the behavior of the algorithm is
273 influenced by numerous parameters of varying importance, starting from the
274 discretization length (element size) or the domain extent, to the limits of the
275 step size τ , the regularization length, or the number of iterations allowed by
276 the line search. A systematic study of each of these parameters would be
277 beneficial in assessing the quality of the shape inferred.

278 Exploring a way to quantify the uncertainty of the answer is also crucial.
279 For example, a sensitivity analysis approach could be considered, as well as
280 the inclusion of a probabilistic quantity.

281 6 Conclusion

282 The present study has successfully demonstrated the application of inverse
283 problems and computational methods to infer the shape of a magma domain
284 beneath a volcano using ground inflation data from satellite observations.
285 The shape optimization technique used in this research showed a new way to
286 identify the most likely shape of the magma chamber. It was intended as an
287 opening to new methods rather than a complete solution.

288 We have shown that modifying a shape optimization algorithm to handle
289 geophysical problems is feasible and of interest. Tests on synthetic data
290 showed to some extent the relevance of the approach, although the best
291 sources found exposed the limitations faced by these first attempts of shape
292 optimization for volcano geodesy. The test on real data showed a concrete
293 case of how the method could be used after being more mature.

294 The perspectives are numerous. The numerical nature of the models
295 allows to easily add complexities to the modeling, such as complex mechanical
296 behavior of the crust (plaxticity, viscoelasticity, poroelsaticity), additional
297 loads (tectonic stress, tidal loads, glacier weights), or inhomogeneities. We
298 hope that the open source code `magmaOpt` developed by us will be modified
299 and extended by future work.

300 By addressing these limitations and extending this approach, researchers
301 can further improve the accuracy and reliability of magma domain shape
302 inference. Ultimately, the development of more sophisticated models will
303 enable geophysicists to better monitor volcanic activity, predict eruptions,
304 and provide critical support for hazard mitigation strategies.

305 References

- 306 Allaire, Grégoire, Charles Dapogny, and François Jouve (2021). “Chapter 1
307 - Shape and Topology Optimization”. In: *Geometric Partial Differential
308 Equations - Part II*. Ed. by Andrea Bonito and Ricardo H. Nochetto.
309 Vol. 22. Handbook of Numerical Analysis. Elsevier, pp. 1–132. DOI: 10.
310 1016/bs.hna.2020.10.004. URL: <https://www.sciencedirect.com/science/article/pii/S1570865920300181>.

- 312 Andreassen, Erik et al. (Jan. 2011). "Efficient Topology Optimization in
313 MATLAB Using 88 Lines of Code". In: *Structural and Multidisciplinary*
314 *Optimization* 43.1, pp. 1–16. ISSN: 1615-147X, 1615-1488. DOI: 10.1007/
315 s00158-010-0594-7. URL: <http://link.springer.com/10.1007/s00158-010-0594-7> (visited on 08/22/2024).
- 316
- 317 Bagnardi, Marco and Andrew Hooper (July 2018). "Inversion of Surface De-
318 formation Data for Rapid Estimates of Source Parameters and Uncer-
319 tainties: A Bayesian Approach". In: *Geochemistry, Geophysics, Geosys-*
320 *tems* 19.7, pp. 2194–2211. ISSN: 1525-2027, 1525-2027. DOI: 10.1029/
321 2018GC007585. URL: <https://agupubs.onlinelibrary.wiley.com/doi/10.1029/2018GC007585> (visited on 02/29/2024).
- 322
- 323 Beghini, Lauren L. et al. (Feb. 1, 2014). "Connecting Architecture and En-
324 gineering through Structural Topology Optimization". In: *Engineering*
325 *Structures* 59, pp. 716–726. ISSN: 0141-0296. DOI: 10.1016/j.engstruct.
326 2013.10.032. URL: <https://www.sciencedirect.com/science/article/pii/S0141029613005014> (visited on 08/21/2024).
- 327
- 328 Bendsøe, Martin P. and Ole Sigmund (2004). "Topology Optimization by
329 Distribution of Isotropic Material". In: *Topology Optimization: Theory,*
330 *Methods, and Applications*. Ed. by Martin P. Bendsøe and Ole Sigmund.
331 Berlin, Heidelberg: Springer, pp. 1–69. ISBN: 978-3-662-05086-6. DOI: 10.
332 1007/978-3-662-05086-6_1. URL: https://doi.org/10.1007/978-3-662-05086-6_1 (visited on 08/21/2024).
- 333
- 334 Cea, Jean (1986). "Conception Optimale Ou Identification de Formes, Calcul
335 Rapide de La Dérivée Directionnelle de La Fonction Coût". In: *ESAIM:*
336 *Modélisation mathématique et analyse numérique* 20.3, pp. 371–402. ISSN:
337 1290-3841. URL: http://www.numdam.org/item/M2AN_1986__20_3_371_0/ (visited on 08/22/2024).
- 338
- 339 Cervelli, P. et al. (2001). "Estimating Source Parameters from Deformation
340 Data, with an Application to the March 1997 Earthquake Swarm off the
341 Izu Peninsula, Japan". In: *Journal of Geophysical Research: Solid Earth*
342 106.B6, pp. 11217–11237. ISSN: 2156-2202. DOI: 10.1029/2000JB900399.
343 URL: <https://onlinelibrary.wiley.com/doi/abs/10.1029/2000JB900399>
344 (visited on 08/22/2024).
- 345
- 346 Charco, M. and P. Galán del Sastre (Mar. 1, 2014). "Efficient Inversion of
347 Three-Dimensional Finite Element Models of Volcano Deformation". In:
348 *Geophysical Journal International* 196.3, pp. 1441–1454. ISSN: 0956-540X.
349 DOI: 10.1093/gji/ggt490. URL: <https://doi.org/10.1093/gji/ggt490> (visited on 08/22/2024).
- 350
- 351 Dapogny, Charles and Eric Bonnetier (2024). *An Introduction to Shape and*
352 *Topology Optimization*. URL: <https://membres-ljk.imag.fr/Charles.Dapogny/coursoptim.html> (visited on 08/21/2024).

- 353 Dapogny, Charles and Florian Feppon (Oct. 31, 2023). “Shape Optimiza-
 354 tion Using a Level Set Based Mesh Evolution Method: An Overview and
 355 Tutorial”. In: *Comptes Rendus. Mathématique* 361.G8, pp. 1267–1332.
 356 ISSN: 1778-3569. DOI: 10.5802/crmath.498. URL: <https://comptes-rendus.academie-sciences.fr/mathematique/articles/10.5802/crmath.498/> (visited on 08/02/2024).
- 359 — (July 30, 2024). *Dapogny/Sotuto*. URL: <https://github.com/dapogny/sotuto> (visited on 08/21/2024).
- 361 Dzurisin, Daniel (2007). *Volcano Deformation: Geodetic Monitoring Tech-
 362 niques*. Springer-Praxis Books in Geophysical Sciences. Berlin ; New York
 363 : Chichester, UK: Springer ; Praxis. 441 pp. ISBN: 978-3-540-42642-4.
- 364 Feppon, F. et al. (Sept. 15, 2020). “Topology Optimization of Thermal Fluid–Structure
 365 Systems Using Body-Fitted Meshes and Parallel Computing”. In: *Jour-
 366 nal of Computational Physics* 417, p. 109574. ISSN: 0021-9991. DOI: 10.
 367 1016/j.jcp.2020.109574. URL: <https://www.sciencedirect.com/science/article/pii/S002199912030348X> (visited on 08/22/2024).
- 369 Frei, Walter (Dec. 29, 2015). *Designing New Structures with Shape Optimiza-
 370 tion*. COMSOL. URL: <https://www.comsol.com/blogs/designing-new-structures-with-shape-optimization> (visited on 08/22/2024).
- 372 Geuzaine, Christophe, Jean-Francois Remacle, and P Dular (2009). “Gmsh:
 373 A Three-Dimensional Finite Element Mesh Generator”. In: *International
 374 Journal for Numerical Methods in Engineering* 79.11, pp. 1309–1331.
- 375 Greiner, Sonja HM (2021). “Including Topography and a 3D-elastic Structure
 376 into a Finite-Element Deformation Model of Grímsvötn, Iceland”. PhD
 377 thesis. URL: <http://hdl.handle.net/1946/38435>.
- 378 Hadamard, J. (1908). *Mémoire Sur Le Problème d’analyse Relatif a l’équilibre
 379 Des Plaques Élastiques Encastrées*. Académie Des Sciences. Mémoires.
 380 Imprimerie nationale. URL: <https://books.google.co.ma/books?id=8wSUmAEACAAJ>.
- 382 Hecht, F. (2012). “New Development in FreeFem++”. In: *Journal of Nu-
 383 matical Mathematics* 20.3-4, pp. 251–265. ISSN: 1570-2820. URL: <https://freefem.org/>.
- 385 Hickey, James and Joachim Gottsmann (June 2014). “Benchmarking and De-
 386 veloping Numerical Finite Element Models of Volcanic Deformation”. In:
 387 *Journal of Volcanology and Geothermal Research* 280, pp. 126–130. ISSN:
 388 03770273. DOI: 10.1016/j.jvolgeores.2014.05.011. URL: <https://linkinghub.elsevier.com/retrieve/pii/S037702731400153X> (vis-
 390 ited on 02/29/2024).
- 391 Hunter, William et al. (2017). *ToPy - Topology Optimization with Python*.
 392 GitHub. URL: <https://github.com/williamhunter/topy>.

- 393 Le Quilliec, Guenael (2014). "Topology Optimization Procedure TOPOP-
394 TIM and Other Various Developments Made with Cast3M". In: DOI:
395 10 . 13140 / 2 . 1 . 2718 . 3682. URL: <http://rgdoi.net/10.13140/2.1.2718.3682> (visited on 02/29/2024).
- 396
- 397 McTigue, D. F. (Nov. 10, 1987). "Elastic Stress and Deformation near a Fi-
398 nite Spherical Magma Body: Resolution of the Point Source Paradox". In: *Journal of Geophysical Research: Solid Earth* 92.B12, pp. 12931–
399 12940. ISSN: 0148-0227. DOI: 10.1029/JB092iB12p12931. URL: <https://agupubs.onlinelibrary.wiley.com/doi/10.1029/JB092iB12p12931> (visited on 02/27/2024).
- 400
- 401
- 402
- 403 Mogi, Kiyoo (1958). "Relations between the Eruptions of Various Volcanoes
404 and the Deformations of the Ground Surfaces around Them". In: *Earthq
405 Res Inst* 36, pp. 99–134.
- 406 Parks, Michelle et al. (Jan. 23, 2024). "Data and Geodetic Modelling Results
407 for Science Article "Fracturing and Tectonic Stress Drives Ultra-Rapid
408 Magma Flow into Dikes"". In: URL: <https://osf.io/9rcq7/> (visited on
409 08/21/2024).
- 410 Sigmund, O. (Apr. 1, 2001). "A 99 Line Topology Optimization Code Writ-
411 ten in Matlab". In: *Structural and Multidisciplinary Optimization* 21.2,
412 pp. 120–127. ISSN: 1615-1488. DOI: 10.1007/s001580050176. URL: <https://doi.org/10.1007/s001580050176> (visited on 08/22/2024).
- 413
- 414 Sigmund, Ole and Kurt Maute (Dec. 1, 2013). "Topology Optimization Ap-
415 proaches". In: *Structural and Multidisciplinary Optimization* 48.6, pp. 1031–
416 1055. ISSN: 1615-1488. DOI: 10.1007/s00158-013-0978-6. URL: <https://doi.org/10.1007/s00158-013-0978-6> (visited on 08/21/2024).
- 417
- 418 Sigmundsson, Freysteinn et al. (Mar. 15, 2024). "Fracturing and Tectonic
419 Stress Drive Ultrarapid Magma Flow into Dikes". In: *Science* 383.6688,
420 pp. 1228–1235. DOI: 10.1126/science.adn2838. URL: <https://www.science.org/doi/10.1126/science.adn2838> (visited on 08/21/2024).
- 421
- 422 Slavov, Stoyan and Mariya Konsulova-Bakalova (Jan. 15, 2019). "Optimizing
423 Weight of Housing Elements of Two-stage Reducer by Using the Topology
424 Management Optimization Capabilities Integrated in SOLIDWORKS: A
425 Case Study". In: *Machines* 7.1, p. 9. ISSN: 2075-1702. DOI: 10.3390/
426 machines7010009. URL: <https://www.mdpi.com/2075-1702/7/1/9>
427 (visited on 08/22/2024).
- 428
- 429 Taylor, Nicola C., Jessica H. Johnson, and Richard A. Herd (Nov. 1, 2021).
430 "Making the Most of the Mogi Model: Size Matters". In: *Journal of
431 Volcanology and Geothermal Research* 419, p. 107380. ISSN: 0377-0273.
432 DOI: 10.1016/j.jvolgeores.2021.107380. URL: <https://www.sciencedirect.com/science/article/pii/S0377027321002092> (vis-
433 ited on 08/22/2024).

- 434 Trasatti, Elisa (July 1, 2022). “Volcanic and Seismic Source Modeling: An
435 Open Tool for Geodetic Data Modeling”. In: *Frontiers in Earth Science*
436 10. ISSN: 2296-6463. DOI: 10.3389/feart.2022.917222. URL: <https://www.frontiersin.org/journals/earth-science/articles/10.3389/feart.2022.917222/full> (visited on 08/21/2024).
- 437 Velez, Maria Laura et al. (Apr. 30, 2011). “Deformation of Copahue Vol-
438 cano: Inversion of InSAR Data Using a Genetic Algorithm”. In: *Journal*
439 of *Volcanology and Geothermal Research* 202.1, pp. 117–126. ISSN: 0377-
440 0273. DOI: 10.1016/j.jvolgeores.2011.01.012. URL: <https://www.sciencedirect.com/science/article/pii/S0377027311000394>
441 (visited on 08/22/2024).
- 442 Yang, Xue-Min, Paul M. Davis, and James H. Dieterich (1988). “Deforma-
443 tion from Inflation of a Dipping Finite Prolate Spheroid in an Elastic
444 Half-Space as a Model for Volcanic Stressing”. In: *Journal of Geophys-
445 ical Research: Solid Earth* 93.B5, pp. 4249–4257. ISSN: 2156-2202. DOI:
446 10.1029/JB093iB05p04249. URL: <https://onlinelibrary.wiley.com/doi/abs/10.1029/JB093iB05p04249> (visited on 08/22/2024).
- 447
- 448
- 449
- 450